CrossMark
click for updates

View Article Online
View Journal

Nanoscale

Accepted Manuscript

This article can be cited before page numbers have been issued, to do this please use: P. Pandey, T. Das, R. Rana, J. B. Parmar, S. Bhattacharyya and D. S. Rana, *Nanoscale*, 2015, DOI:

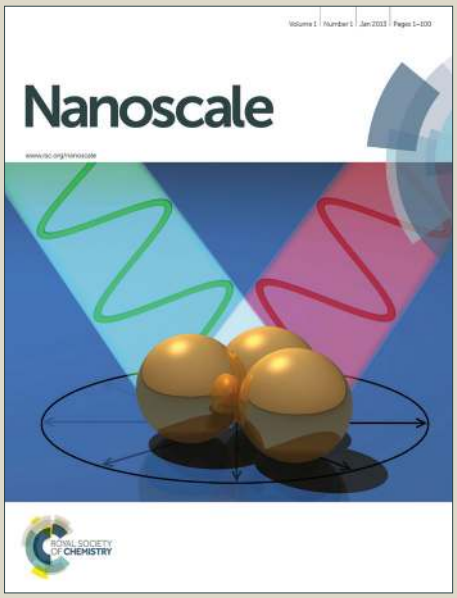

This is an *Accepted Manuscript*, which has been through the Royal Society of Chemistry peer review process and has been accepted for publication.

Accepted Manuscripts are published online shortly after acceptance, before technical editing, formatting and proof reading. Using this free service, authors can make their results available to the community, in citable form, before we publish the edited article. We will replace this *Accepted Manuscript* with the edited and formatted *Advance Article* as soon as it is available.

You can find more information about *Accepted Manuscripts* in the Information for Authors.

Please note that technical editing may introduce minor changes to the text and/or graphics, which may alter content. The journal's standard Terms & Conditions and the Ethical guidelines still apply. In no event shall the Royal Society of Chemistry be held responsible for any errors or omissions in this *Accepted Manuscript* or any consequences arising from the use of any information it contains.

ROYAL SOCIETY OF CHEMISTRY

www.rsc.org/nanoscale

View Article Online
DOI: 10.1039/C4NR07314B

Electronic control of interface ferromagnetic order and exchange-bias in paramagnetic-antiferromagnetic epitaxial bilayers

Parul Pandey[1§], Tanmay Das[2§], Rakesh Rana[1], J. B. Parmar[2], S. Bhattacharyya[2], D. S. Rana[1]**

[1]*Department of Physics, Indian Institute of Science Education and Research Bhopal, Govindpura, Bhopal-462023, India*

[2]*DCMP&MS, Tata Institute for Fundamental Research, Dr Homi Bhabha Road, Colaba, Mumbai-400 005, India*

[§]Equal contribution

*dsrana@iiserb.ac.in, somnath@tifr.res.in

The hetero-epitaxial engineered novel magnetic phases, formed due to entanglement of the spin, charge and lattice degrees of freedom, at the atomically sharp interfaces of complex oxides heterostructures are indispensable for devising the multifunctional devices. In a quest for novel and superior spintronics functionalities, we have explored the interface magnetism in the epitaxial bilayer of atypical magnetic and electronic states, *i.e.*, of paramagnetic metallic and antiferromagnetic (AFM) insulating phases. In this framework, we observe an unusually strong ferromagnetic order and large exchange-bias fields generated at the interface of the bilayers of metallic $CaRuO_3$ and AFM insulating manganite. The magnetic moment of the interface ferromagnetic order increases linearly with the increasing thickness (7 – 90 nm) of the metallic $CaRuO_3$ layer. This linear scaling signifying an electronic (non-magnetic) control of the interface magnetism and a non-monotonic dependence of the exchange-bias on metallic layer evlove as novel spintronics attributes in atypical bilayers.

Published on 12 January 2015. Downloaded by Selcuk University on 14/01/2015 15:24:18.

Nanoscale Accepted Manuscript

View Article Online
DOI: 10.1039/C4NR07314B

Published on 12 January 2015. Downloaded by Selcuk University on 14/01/2015 15:24:18.

Formation of exotic electronic and magnetic phases at the atomically sharp interfaces has attracted immense interest in the contemporary research on epitaxial engineered superlattices.[1-4] These phases manifest due to dissimilar magnetic and electronic structures of constituent layers of the superlattice. The 2D electron gas in the multilayers of band- and correlated-insulator[5,6] and the interface superconductivity in the metal–insulator (or metal) bilayers[7,8] are remarkable examples of interface electronic phases. Their formation by the orbital and electronic structure reconstruction at the interfaces is widely accepted. However, the control of interface phases by seemingly less relevant properties of the constituent layers is far more intriguing. For instance, an insulating layer thickness control of the interface superconductivity in insulator-metal bilayers is the most astounding discovery. [7,8] Another domain in interface physics is of magnetism which holds immense potential for technological applications. In this context, the interface ferromagnetic (FM) order and the exchange-bias fields (H_{EB}) are the major attributes to derive the spintronics applications.[9-13] Obtaining and controlling these interface magnetic properties by unconventional methods is critical to the quest for a novel fundamental paradigm and flexible spintronics functionality. In view of this, the interface magnetism in non-magnetic phases and its control by non-magnetic elements, analogous to the insulating layer control of superconductivity in insulator-metal bilayers, are highly desired characteristics.

In this communication, we present an electronic (non-magnetic) control of the interface magnetism and exchange-bias in the epitaxial bilayers of the metallic paramagnetic (PM) and insulating antiferromagnetic (AFM) systems. The 3d- and 4d-transition metal oxides exhibit a variety of electronic structures and correlations that are promising for interface reconstruction. Hence, an epitaxial growth of bilayers of the 4d-oxide $CaRuO_3$ (PM-metallic) and the 3d-magnetically ordered manganites, i.e., of the weekly and strongly correlated systems, was contemplated to yield novel interface phases.[2,3,10] We present the observation of an unusually strong FM order and the unconventional exchange-bias fields generated at the interfaces of the epitaxial bilayers of PM-metallic $CaRuO_3$ (CRO) and AFM insulating $Eu_{0.42}Sr_{0.58}MnO_3$ (ESMO).[14,15] Above all, we demonstrate the scaling of interface FM order and exchange bias with the thickness of the metallic CRO layer, which signifies an electronic control of the interface magnetism.

Nanoscale Accepted Manuscript

View Article Online
DOI: 10.1039/C4NR07314B

Published on 12 January 2015. Downloaded by Selcuk University on 14/01/2015 15:24:18.

The compressive strained ESMO/CRO bilayers were formed on $LaAlO_3$ [LAO] (100) substrate. Two series of samples, namely, i) $ESMO_{90}/CRO_n$ bilayers with same thickness of ESMO (~90 nm) layer but different CRO layer thickness (n~7–90 nm), and, ii) $ESMO_m/CRO_{15}$ bilayers with same CRO layer thickness (~15 nm) but different ESMO layer thickness (m ~ 15-120 nm). A multilayer $ESMO_5/CRO_2$ having 10 layer repetitions was also formed for the sake of comparison with the bilayers [subscript denotes the thickness of corresponding layer]. The bottom layer of ESMO was chosen primarily due to its robust charge-ordered AFM state and its lattice match with CRO which prevents any additional epitaxial strain. Also, the deposition of ESMO/CRO on LAO (100) renders the bilayer in compressive strain, thus, ensuring a PM metallic phase of the CRO layer. All the bilayers were deposited on LAO (100) single crystal substrate by pulsed laser deposition technique, using a 248 nm Excimer laser. X-ray diffraction studies were carried out using a powder diffractometer acquainted with 4-axis cradle. Magnetization measurements were performed on a SQUID magnetometer. Electrical resistivity and Hall effect measurements were performed in a PPMS (Quantum Design). To study the interface quality at atomic level scanning transmission electron microscopic (STEM) experiments were carried out using a FEI-TITAN microscope operated at 300 kV equipped with FEG source, Cs (spherical aberration coefficient) corrector for condenser lens systems and a high angle annular dark field (HAADF) detector.

All the bilayer films are phase-pure and epitaxial. The x-ray patterns show only one peak for both CRO and ESMO layers corresponding to each LAO peak (Figure 1a), which suggests a strong structural coupling between the two layers. The x-ray reflectivity measurements performed on $ESMO_{15}/CRO_{15}$ sample (Figure 1b) clearly depicts two main fringes and their repetitive fringes. Of the two main fringes, one fringe corresponds to the ESMO layer and the other is for CRO layer. This suggests sharp interfaces in the bilayers. The reciprocal space maps (RSM) recorded along the asymmetric (301) and (311) reflections of LAO (Figure 1c) reveal that peaks of both the layers lie on the pseudomorphic line of the LAO substrate. This suggests same in-plane lattice parameters of the bilayer and the substrate (3.79 Å). Also, a single peak corresponding to these two layers confirms nearly same out-of-plane parameter for both the CRO and the ESMO layers (Figure 1a and c).

Nanoscale Accepted Manuscript

View Article Online
DOI: 10.1039/C4NR07314B

Published on 12 January 2015. Downloaded by Selcuk University on 14/01/2015 15:24:18.

To further investigate the quality of the interfaces, STEM measurements using HAADF detector were performed on some representative bilayers. High resolution HAADF-STEM images of the LAO/ESMO and the ESMO/CRO interfaces for the $ESMO_{90}/CRO_{15}$ and $ESMO_{90}/CRO_7$ bilayers are presented in Figure 2a-d. The positions of the different projected atomic columns along the viewing direction are indicated in LAO/ESMO and ESMO/CRO interfaces of $ESMO_{90}/CRO_{15}$ bilayer with different coloured circles (Figure 2a andb). The schematics of the respective crystal structures projected along the viewing direction <110> are shown in the insets. In a HAADF-STEM image, the intensity (I) is proportional to Z^2 (Z= atomic number), *i.e*, the variation of intensity in imaged region gives information on compositional changes across the interface. Comparison of the schematic (the inset) with the image in Figure 2a gives an indication of the presence of sharp LAO/ESMO interface in the $ESMO_{90}/CRO_{15}$ bilayer. To measure it quantitatively 1D line scans across the interface were taken. One of the line scans, taken from the dotted box of Figure 2a and presented in Figure 2e, consists a decaying background which is characteristic of wedge shaped TEM samples. Here, the area under curves above the background was considered for calculation. As projected atomic columns of La in LAO side of the interfaces are facing the projected atomic columns of Sr/Eu in ESMO side, *i.e*, the calculated intensity ratio in the HAADF-STEM image (I_{La} / $I_{Sr/Eu}$) is 1.4 (average Z was used as per composition of Eu/Sr). The ratio of the areas under the curves in LAO and ESMO side of the interface in Figure 2e agrees well with the calculated value. This proves that no diffusion occurs through this interface.

Now, we analyse the interface quality of ESMO and CRO layers. Comparison of the schematic with the image in Figure 2b gives an indication of the presence of sharp ESMO/CRO interface in the $ESMO_{90}/CRO_{15}$ bilayer. The image of ESMO/CRO interface shows half unit-cell shift between the bright features in either side of the interface. This is because Sr/Eu in ESMO and Ru in CRO are the elements with large Z and there is half unit-cell shift in their projected position parallel to the viewing direction (as shown in the schematic). Two of the 1D line scans taken from the dotted boxes 1 and 2 in Figure 2b are presented as Figure 2f and g, respectively. According to the schematic (inset Figure 2b), the projected atomic columns containing Sr/Eu in ESMO side face the projected atomic columns containing Ca in CRO side of the interface. In Figure 2f, it is noted that the area under the curve of only one Sr/Eu atomic column, which is closest to the interface, differs slightly from the rest in ESMO side. The ratio of the area under

Nanoscale Accepted Manuscript

View Article Online
DOI: 10.1039/C4NR07314B

Published on 12 January 2015. Downloaded by Selcuk University on 14/01/2015 15:24:18.

the curves (other than one atomic column at the interface in ESMO side) in ESMO and CRO side in Figure 2f is around ~4 which agree well with the calculated intensity ratio of the HAADF-STEM image ($I_{Sr/Eu}/I_{Ca}$) from the ratio of Z^2 values. Overall, it can be stated that no signature of any discernible chemical diffusion of Ca and Sr was found. Similar analysis was performed to explore the possibility of chemical inter-diffusion of Ru and Mn. As per schematic in inset Figure 2b, the atomic columns with a mixture of 1/3 of Mn and 2/3 of O on ESMO side face the atomic columns with 1/3 of Ru and 2/3 of O on CRO side of the interface. Figure 2g shows 1D line scans for this analysis. Here the ratio of the area under the curves (other than one atomic column at the interface in CRO side) in CRO and ESMO side of the interface (Figure 2g) is around ~2.2 which agrees well with the calculated intensity ratio of the HAADF-STEM image ($I_{Ru/O}/I_{Mn/O}$) from the ratio of Z^2 values (where Ru:O=0.33:0.67, Mn:O=0.33:0.67). So, it can be stated that no signatures of chemical diffusion of Mn and Ru was found. A mixing in one interface layer, in both the case of Ca and Sr and Mn and Ru may be attributed to visibly evident step-like behaviour of unit-cell size arising from the surface/interface roughness. The $ESMO_{90}/CRO_7$ bilayer too exhibit similar behaviour with reasonably sharp interface quality.

The temperature dependence of magnetization reveals the onset of a FM order in a broad temperature range 80-120 K and a pronounced bifurcation of zero-field-cooled and field-cooed magnetization at ~50 K (inset Figure 3c). The magnetization versus magnetic-field isotherms for all the $ESMO_{90}/CRO_n$, $[CRO_2/ESMO_5]_{10}$ multilayer, and $ESMO_m/CRO_{15}$ bilayers at 10 K reveal a FM hysteresis loops (Figure 3a and b). The FM hysteretic loops seen in these samples is not a property of either the CRO layer or the ESMO layer, as both these layers when deposited alone on LAO (100) substrate do not display any signatures of FM order. This behavior can be attributed to two key factors, namely, the chemical interdiffusions resulting in doping Sr at Ca in $CaRuO_3$ layer and the interface FM order at the chemical sharp interfaces of the bilayer. First, with the following experimental evidences and arguments, we discard the possibility of chemical interdiffusion. The most relevant chemical inter-diffusion is of Ca and Sr at the interface. However, as clearly depicted by x-ray reflectivity data and the analysis of STEM data, the inter-diffusion of Ca and Sr is not a dominant feature which can alter the interface magnetism (Figure 1b and Figure 2). The possibility of chemical interdiffusion at the interface of ESMO-CRO bilayers is further discarded with th following data. We have deposited two bilayers, similar to

Nanoscale Accepted Manuscript

View Article Online
DOI: 10.1039/C4NR07314B

Published on 12 January 2015. Downloaded by Selcuk University on 14/01/2015 15:24:18.

ESMO-CRO, but with no relevance of Ca and Sr interdiffusion. These are; i) $CaMnO_3$ (CMO ~ 90 nm) with CRO (30 nm) [having only Ca in both the layers] and ii) ESMO (90 nm) $SrRuO_3$ (SRO ~ 7nm) [having only Sr in both the layers]. The magnetization of these samples is shown in inset Figure 3d. Clearly, the magnetic moment of CMO_{90}/CRO_{30} bilayer is quite similar to its $ESMO_{90}/CRO_{30}$ counterpart (Figure 3a). The magnetic moment of SRO based ($ESMO_{90}/SRO_7$), however, is much larger than that of that of the $ESMO_{90}/CRO_7$ bilayer (Figure 3a). This is becuase SRO is FM phase which has a saturation magnetization of SRO is ~ $2\mu_B$/Ru-site. But it is noted that the magnetic moment of this bilayer is twice than that can be accounted by a 7nm SRO layer. In fact, the subtraction of SRO moment results in the interfacial moments equal to that of the $ESMO_{90}/CRO_7$ bilayer. Overall, the magntization behavior of both the CMO/CRO and ESMO/SRO is similar to that their ESMO/CRO counterparts. This, along with the reflectivity data, STEM data and paramagnetic nature of compressive CRO, clearly suggest that the magnetic moment of all these samples is not a result of chemical interdiffusion.

Now, we consider and understand the unusual FM order of ESMO/CRO bilayers in context of interface effect. These data exhibit two remarkable features. One, the magnetic moment in the bilayers is too large to be accounted by one or two unit-cell layers at the interface. This assertion is based on the fact that even the magnetic moment of the $[ESMO_5/CRO_2]_{10}$ multilayer (having ten interfaces) is lesser than the moment of some bilayers (Figure 3a). This suggests that the interface FM layer in the bilayers extends itself beyond the chemical interface deep up to 5-10 unit cells into the ESMO layer.[9] Two, the magnetization scales linearly with the thickness of the top PM metallic CRO layer; the magnetic moment increases by more than one order of magnitude as the CRO layer thickness increases from 7 nm to 90 nm (Figure 3c). The magnetization as a function of the ESMO layer thickness, *i.e*, for $ESMO_m/CRO_{15}$ (m = 120, 90, 25 and 15 nm) bilayers, was also studied (Figure 3b). The magnetization decreases with decreasing 'm' up to a thickness of 25 nm but this trend is arrested at m=15 nm. In this sample, the moment increases marginally compared to that for 25 nm ESMO layer, which may be attributed to the fact the robustness of AFM order in charge-ordered ESMO layer collapses at lower thickness (15 nm) and the competing FM order dominates.

Comparing the magnetization of two series of ESMO/CRO samples, it is noteworthy that for a similar variation of the thickness of ESMO and CRO, the magnetization exhibits a pronounced

Nanoscale Accepted Manuscript

View Article Online
DOI: 10.1039/C4NR07314B

Published on 12 January 2015. Downloaded by Selcuk University on 14/01/2015 15:24:18.

increase of one order of magnitude as a function of CRO layer thickness vis-a-vis an increase of only two factors in case of variation of ESMO thickness (Figure 3c and inset Figure 3b). This interface FM order was evaluated by established models. The critical field (H_C) of the FM loops decays exponentially with temperature, as per the phenomenological equation [9,12]

$$H_C(T) = H_C^0 e^{(-T/T_A)} \quad (1)$$

where, H_C^0 is the extrapolation of coercivity at 0 K and T_A is a constant. This behaviour, as shown for a typical $ESMO_{90}/CRO_{30}$ sample in figure 3d, is reminiscent of the frustrated spins present at the FM-AFM interfaces of the bilayers.[16] An H_C^0 = 0.11 T and T_A = 18.1 obtained from the fits of PM-AFM $ESMO_{90}/CRO_{30}$ bilayers suggest a disordered interface, which is generally observed in FM and AFM heterostructures.[17] This implies presence of an interface FM layer which is in contact with AFM ESMO layer.

A strong interface FM order in contact with AFM layer can induce some fascinating exchange-bias fields. This aspect was explored for all the $ESMO_{90}/CRO_n$ and the $ESMO_m/CRO_{15}$ bilayers. Figure 4a-d shows these data of some representative samples acquired upon cooling in a field of ±7 T. All the samples exhibit negative exchange-bias effect as is evident from the shifting of centre of magnetic loop in the direction opposite to the direction of the magnetic field; a property typical of FM-AFM hetero-structures. On one hand, the exchange-bias does not follow a linear trend with the thickness of CRO layer. The exchange bias field (H_{EB}) increases with CRO layer thickness up to n = 45 nm, beyond which it saturates (Figure 4e). This is unexpected because the exchange-bias in the conventional FM-AFM structures increases with decreasing thickness of the FM layer.[12,13,18] On the other hand, the H_{EB} in $ESMO_m/CRO_{15}$ exhibits the expected behavior; it decreases (Figure 4f) with decreasing thickness of the AFM ESMO layer. [18] The H_{EB} nearly vanishes for m=15 nm which clearly suggests either very weak AFM order or low thickness of ESMO is insufficient to couple with the cooling field (Figure 4d).

The H_{EB} behavior further analyzed with respect to the cooling field (H_{CF}) and the temperature. Figure 4g and the inset reveal that both the H_{EB} and H_C increase with the increasing H_{CF}, respectively. Also, the H_{EB} decreases on increasing the temperature of $ESMO_{90}/CRO_{30}$ and vanishes in the vicinity of 70-80 K (inset Figure 4h), which is referred to as the blocking

Nanoscale Accepted Manuscript

View Article Online
DOI: 10.1039/C4NR07314B

Published on 12 January 2015. Downloaded by Selcuk University on 14/01/2015 15:24:18.

temperature above which the magnetic order (consequently exchange-bias effect) ceases to exist.[12,13]Here, the blocking temperature of ~80 K seems to originate from the FM order in ESMO. In the phase diagram of $Eu_{1-x}Sr_xMnO_3$, a long range FM order with Curie temperature of ~80 K manifests for x=0.40-0.48.[14,15] This suggests a direct correspondence of FM ordering and blocking temperature. In present case of bilayers the x=0.58 ESMO composition is a robust AFM phase. To induce FM order in this system, it requires injection of electrons to obtain x = 0.40-0.48 stoichiometry [to be discussed later]. Typically, the H_{EB} is accompanied by its corresponding H_C,[12,13] both of which decay exponentially with increasing temperature (Figure 4h and inset), as per equation (1) and (2)

$$H_{EB}(T) = H_{EB}^{0} e^{(-T/T_A)} \quad (2)$$

Here, the H_{EB}^{0} and H_C^{0} is the extrapolation of exchange bias and coercive field at 0 K, respectively, and T_A is a constant (Figure 4h and inset).[9,12,13] This also suggests a typical frustrated spin state at the interfaces of FM-AFM layers.[17] Overall, the H_{EB} in ESMO/CRO bilayers shows a typical behaviour with respect to the temperature, cooling-field and thickness of AFM layer. However, the behaviour of exchange bias with respect to the thickness of CRO layer is unusual and cannot be explained in any existing framework.

The large interface magnetic moment extends itself beyond the chemical interface deep down to more than 10 unit cells into the ESMO layer.[10] Other possibility of the FM moment in top layer is ruled out as CRO exhibits a PM ground state under the compressive strain,[19,20] suggesting that the FM moments are induced in the AFM ESMO layer of the bilayer. In charge-ordered manganites, an AFM phase can be transformed to FM phase either via structural modification or by changing the carrier density.[2,14,15] A structural change charge-ordered ESMO phase is ruled out.[14,15] This is evident from the XRD and STEM data which show a uniform structure across the entire ESMO layer. In such a case, the change in carrier concentration is likely to induce the FM order, as follows. The $Eu_{1-x}Sr_xMnO_3$ exhibits FM order, spin-glass phase and AFM order for Mn^{4+} content range (x) of ~ 0.40-0.48, 0.49-0.52 and 0.53-0.60, respectively.[14,15] In present case of ESMO (x=0.58), the FM phase can be induced by increasing Mn^{3+} content (which is 42%) by injecting electrons into it. This can be realised in our bilayers by

Nanoscale Accepted Manuscript

View Article Online
DOI: 10.1039/C4NR07314B

Published on 12 January 2015. Downloaded by Selcuk University on 14/01/2015 15:24:18.

the leakage of electrons from the top metallic CRO layer into the bottom AFM ESMO layer (Figure 5a). It is theoretically shown that the leakage of electrons from the conducting layer is exponential across the interface into the insulating bottom layer.[2] This suggests that on acquiring larger electron density, the few unit cells in the AFM ESMO layer and in the close vicinity of interface might acquire FM order. In this case, the FM moment will arise from more than 1-2 interface layers. As the electron density dies exponentially from the interface into the EMSO layer, it is possible that there will be non-uniform FM order across those layers (Figure 5a). In ESMO/CRO bilayers, a broad FM order in the vicinity of 70-80 K matches well with the FM ordering temperature of the $Eu_{1-x}Sr_xMnO_3$ with x = 0.42 - 0.48 whereas bifurcation of magnetization curves at 50 K is reminiscent of a spin-glass like behaviour for x = 0.49 -0.52 (inset Figure 3c).[14,15] This suggests a gradient in strength of magnetic order in the ESMO layer beneath the interface; a stronger FM order at the interface weakens while traversing from interface to deep into the ESMO layer. This also explains the anomalous variation of H_{EB} with CRO thickness; as the thickness of CRO layer increases, the FM moment increases suggesting a thicker interface layer with a larger gradient in its strength. This will facilitate an easy pinning of a weak FM order beneath the interface. Hence, the H_{EB} increases with increasing thickness of the metallic CRO layer. Thus suggested model (Figure 5a) was implemented to calculate the magnetization per formula unit for the to the assumed FM thickness (proportional to CRO thickness) and is plotted in Figure 5b. The number of FM unit cell layers considered for these calculations increase linearly (from 8 -20) with increasing thickness of CRO layers (Figure 5c). A slight decrease in the magnetization with increasing CRO thickness may be attributed to the larger gradient in strength of FM order down the ESMO thickness.

Now we discuss the electronic control to the interface magnetic order and the exchange bias. The interface FM order of ESMO/CRO bilayers scales linearly with the thickness of the metallic CRO; magnetic moment increases by one order of magnitude as the thickness of CRO is increases from 7 nm to 90 (Figure 3). This unambiguously depicts a whole new concept that the metallicity can control the interface FM order and the exchange bias. This was supported by the electrical properties of all the bilayers (Figure 6). The $ESMO_{90}/CRO_n$ bilayers with n = 7, 15 and 30 nm do not exhibit metallic behaviour but a peculiar insulator-metal transition (Figure 6a and inset). This indicates localization of the carriers on CRO layer as it gets partly depleted of carriers due to leakage of electrons into the bottom layer. Now as the thickness of CRO is

Nanoscale Accepted Manuscript

View Article Online
DOI: 10.1039/C4NR07314B

Published on 12 January 2015. Downloaded by Selcuk University on 14/01/2015 15:24:18.

increased, the ratio of free electrons available in CRO and the electrons leaked increases, thus, revealing a dominant metallic conductivity of CRO with increasing n (Figure 6b). The carrier density obtained from the Hall effect measurement.[21,22] Figure 6c too suggests the same. An increase in carrier density from $\sim$-7×10^{21} / cm^3 for n = 7 nm to $\sim$-1.2×10^{23} / cm^3 for n = 45 nm too suggests the dominant role of leakage of electrons in inducing a large interface FM order.

There are two aspects of the transport properties of these bilayers which deserve detailed discussions, namely, i) the role of interface FM layer on the resistivity of the bilayer and, ii) non-monotonic dependence of resistivity on the thickness of CRO layer of the bilayer. In the former case, the ESMO is expected to be metallic in the FM phase as per the Zener-double-exchange. However, the conductivity of ESMO is 2-3 orders of magnitude lower than that of the CRO phase.[14,21] In the bilayer, the current flows through the less resistive path in the current-in-plane configuration of resistivity measurements. As CRO is the top layer, it offers lesser resistance path compared to that of the ESMO layer. Hence, given the fact that interfacial FM ESMO layers is 2-3 orders of magnitude less conductive compared to that of the top CRO layer, the resistivity as well as Hall-effect measurements of the bilayer will reflect the transport behaviour of CRO only. An obvious effect is the absence of any anomalous Hall component from the high resistive interface FM layer. Now we comment on the latter aspect, *i.e.*, the resistivity depends non-monotonically on the thickness of CRO layer. This is because the interface ESMO need about 0.08-0.13 electrons (leaking from CRO layer) per Mn ion to exhibit a FM or spin-glass like behaviour. So, for thin CRO layers (such as in $ESMO_{90}/CRO_7$), the fraction of the electrons leaked compared to the total electrons available/left with CRO may be a substantial. But as the thickness of CRO layer increases, the number of electrons leaking might become insignificant to that of total electrons in CRO layer. Hence, it is clearly observed that the for bilayers with low CRO thickness, the resistivity of CRO is not its bulk-like property while bilayers with thicker CRO layers exhibit resistivity reminiscent of the bulk CRO property.

The aspect of electronic control of the magnetic order and exchange-bias in unconventional PM-AFM bilayers of ESMO/CRO is a magnetic facet analogous to the remarkable discovery of interface superconductivity in cuprate metal-insulator bilayers, in which the superconductivity was controlled by the thickness of insulating layer.[10] In spintronics, the electrical transport is dependent on the spin-order.[2-4,6] In this context, our work demonstrates a

Nanoscale Accepted Manuscript

View Article Online
DOI: 10.1039/C4NR07314B

Published on 12 January 2015. Downloaded by Selcuk University on 14/01/2015 15:24:18.

new paradigm, *i.e.*, controlling the spin-order by the electronic properties and, thus, created spin-order induces the exchange bias which in turn will realize the spin (magnetic) control of electrical transport. Here, it is imperative to invoke the case of $LaNiO_3/CaMnO_3$ multilayers in which a weak interface FM order manifests only if the top layer $LaNiO_3$ is metallic.[11] In $CaRuO_3/CaMnO_3$ multilayers with atomically sharp interfaces, the FM order manifested only in one interface unit cell layer.[2,3,10] Compared to these studies depicting a presence of only a weak interface FM order, our studies performed on bilayers with a very broad thickness range of both PM/AFM layers show a very large enhancement of magnetic moment and exchange-bias with the thickness of PM metallic layer.

To sum up, the magnetic moment of the FM order at the interface of the metallic PM – insulating AFM bilayers can be increased by about an order of magnitude by increasing the thickness of non-magnetic metallic layer. This emphasizes that volume of the individual layers is very effective in inducing the robust interface magnetic properties, and establishes a unique electronic control of the interface FM order and exchange-bias having implications in spintronics. Remarkably, this study not only evolves a way to induce, enhance and, in fact, tune the interface magnetism by controlling the electrons leaking into the AFM insulating layer from the non-magnetic metallic layer but also shows the fascinating property of a large exchange bias in the unconventional PM-AFM epitaxial bilayers.

Nanoscale Accepted Manuscript

View Article Online
DOI: 10.1039/C4NR07314B

Published on 12 January 2015. Downloaded by Selcuk University on 14/01/2015 15:24:18.

References:

1. H. Y. Hwang, Y. Iwasa, M. Kawasaki, B. Keimer, N. Nagaosa and Y. Tokura, *Nat. Mater.* **(2012)**,11, 103.
2. B. R. K Nanda, S. Satpathy and M. S. Springborg, *Phys. Rev. Lett.* **(2007)**, 98, 216804.
3. J. W. Freeland, J. Chakhalian, A. V. Boris, J.-M. Tonnerre, J. J. Kavich, P. Yordanov, S. Grenier, P. Zschack, E. Karapetrova, P. Popovich, H. N. Lee and B. Keimer, *Phys. Rev. B* **(2010)**, 81, 094414.
4. J. Hoffman, I. C. Tung, B. B. Nelson-Cheeseman, M. Liu, J. W. Freeland and A. Bhattacharya, *Phys. Rev. B* **(2013)**, 88, 144411.
5. S. Thiel, G. Hammerl, A. Schmehl, C. W. Schneider and J. Mannhart, *Science* **(2006)**, 313, 5795.
6. J. Manhart and D.G. Scholm, *Science* **(2010)**, 327, 1607.
7. A. Gozar, G. Logvenov, L. Fitting Kourkoutis, A. T. Bollinger, L. A. Giannuzzi, D. A. Muller, and I. Bozovic, *Nature* **(2008)**, 455, 782.
8. J.Chaloupka and G. Khaliullin, *Phys. Rev. Lett*. **(2008)**, 100, 016404.
9. J. F. Ding, O. I. Lebedev, S. Turner, Y. F. Tian, W. J. Hu, J. W. Seo, C. Panagopoulos, W. Prellier, G. V. Tendeloo and T. Wu, *Phys. Rev. B* **(2013)**, 87, 054428.
10. C. He, A. J. Grutter, M. Gu, N. D. Browning, Y. Takamura, B. J. Kirby, J. A. Borchers, J. W. Kim, M. R. Fitzsimmons, X. Zhai, V. V. Mehta, F. J. Wong and Y. Suzuki, *Phys. Rev. Lett*. **(2012),** 109,197202.
11. A. J. Grutter, H. Yang, B. J. Kirby, M. R. Fitzsimmons, J. A. Aguiar, N. D. Browning, C. A. Jenkins, E. Arenholz, V. V. Mehta, U. S. Alaan and Y. Suzuki, *Phys. Rev. Lett*. **(2013)**, 111,087202.
12. R. Rana, P. Pandey, R. P. Singh, & D. S. Rana, Sci. Rep. **(2014)**, 4, 4138
13. R. Rana, P. Pandey, and D. S. Rana, *Appl. Phys. Lett.* **(2014)**, 104, 092413.
14. Y. Tomioka, R. Kumai, T. Ito, and Y. Tokura, *Phys. Rev. B* **(1997)**, 80, 174414.
15. P. Pandey, N. Awari, R. Rana, A. Singh, S. S. Prabhu and D. S. Rana, *Appl. Phys. Lett.* **(2012)**, 100**,** 062408.
16. K. Maiti, *Phys. Rev. B* **(2006)**, 73, 235110.
17. G. Cao, S. McCall, M. Shepard, J.E. Crow and R.P. Guertin, *Phys. Rev. B* **(1997)**, 56, 321.

Nanoscale Accepted Manuscript

View Article Online
DOI: 10.1039/C4NR07314B

18. J. Nogués, J. Sort, V. Langlais, V. Skumryev, S. Suriñach, J. S. Muñoz and M. D. Baró, *Phys. Rep.* **(2005)**, 422, 65.
19. A. T. Zayak, X. Huang, J. B. Neaton, and K. M. Rabe, *Phys. Rev. B* **(2008)** 77, 214410.
20. S. Tripathi, R. Rana, S. Kumar, P. Pandey, R.S. Singh and D.S. Rana, *Sci. Rep* **(2014)** 4, 3877.
21. M. Ziese, F. Bern, A. Setzer, E. Pippel, D. Hesse, and I. Vrejoiu, *Eur. Phys. J. B* **(2013)**, 86, 1.
22. Parul Pandey, Rakesh Rana, Shivendra Tripathi, and D. S. Rana, *Appl. Phys. Lett.* **(2013)**, 103, 032403.

Published on 12 January 2015. Downloaded by Selcuk University on 14/01/2015 15:24:18.

Nanoscale Accepted Manuscript

View Article Online
DOI: 10.1039/C4NR07314B

Published on 12 January 2015. Downloaded by Selcuk University on 14/01/2015 15:24:18.

Figure 1:

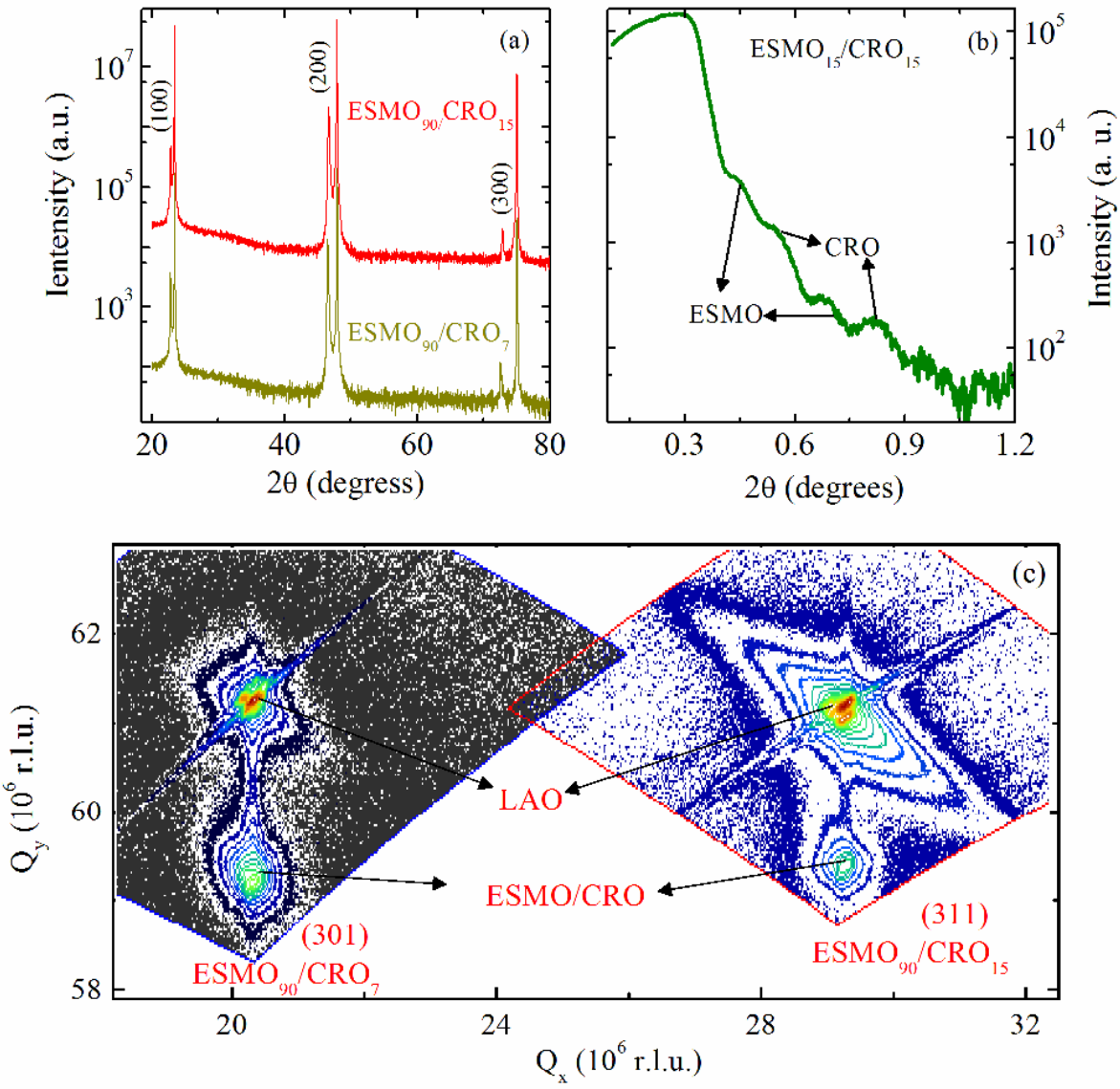

Figure 1: (a & c) X-ray diffraction pattern of $ESMO_{90}/CRO_7$ and $ESMO_{90}/CRO_{15}$ bilayers, respectively. (b) X-ray reflectivity measurements of $ESMO_{15}/CRO_{15}$ bilayer, arrows indicate the reflection of corresponding layer. (c) Reciprocal space maps in reciprocal lattice units (r.l.u.) for $ESMO_{90}/CRO_7$ and $ESMO_{90}/CRO_{15}$ bilayers, respectively

Nanoscale Accepted Manuscript

View Article Online
DOI: 10.1039/C4NR07314B

Published on 12 January 2015. Downloaded by Selcuk University on 14/01/2015 15:24:18.

Figure 2:

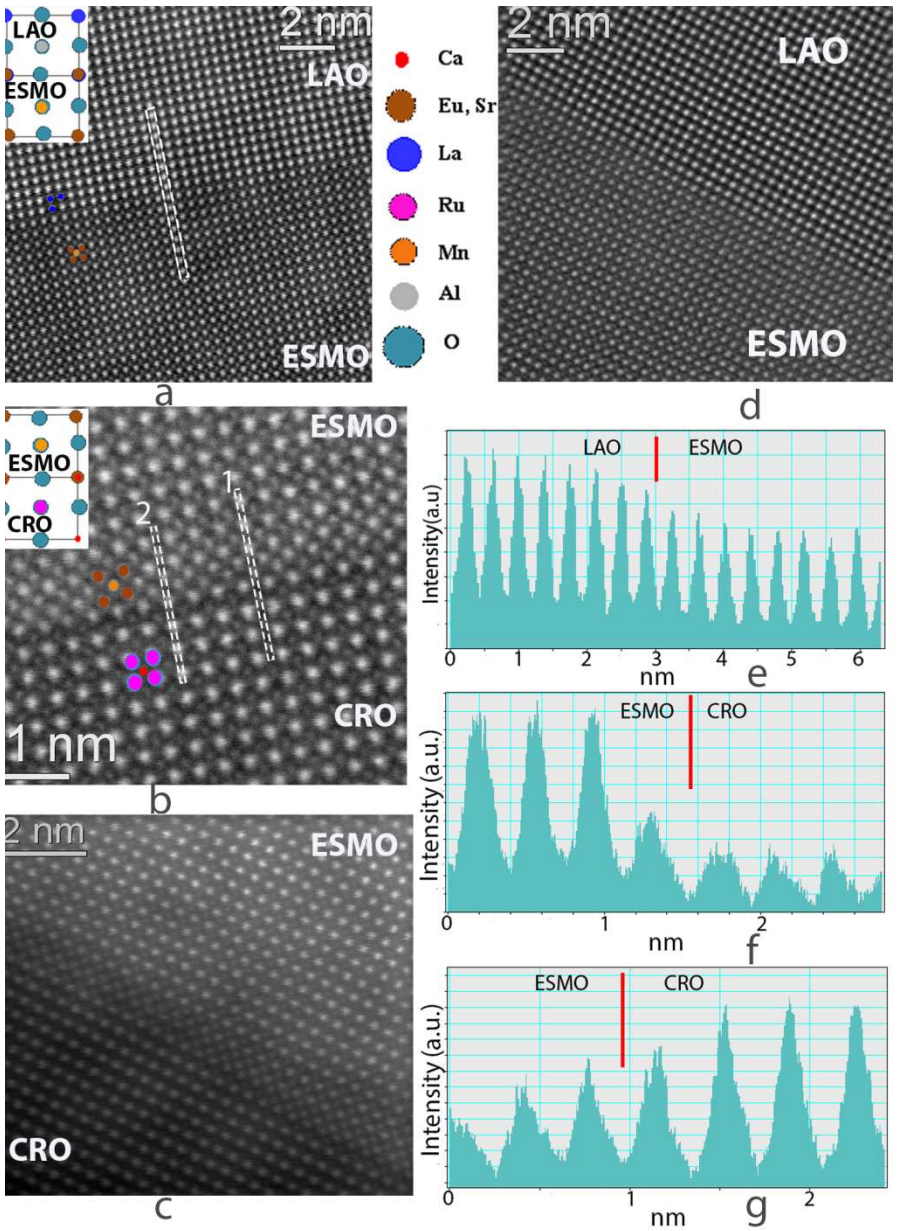

Figure 2: (a-d) HAADF-STEM images of the two samples at high magnifications, (a) and (b) are the LAO/ESMO and ESMO/CRO interfaces, respectively, for $ESMO_{90}/CRO_{15}$ and (c) and (d) are the ESMO/CRO and LAO/ESMO interfaces for $ESMO_{90}/CRO_{7}$ bilayer. (e) 1-D line scans taken from the dotted box of (a). (f) and (g) are the line scans taken from the dotted boxes 1 and 2 of (b).

Nanoscale Accepted Manuscript

View Article Online
DOI: 10.1039/C4NR07314B

Published on 12 January 2015. Downloaded by Selcuk University on 14/01/2015 15:24:18.

Figure 3:

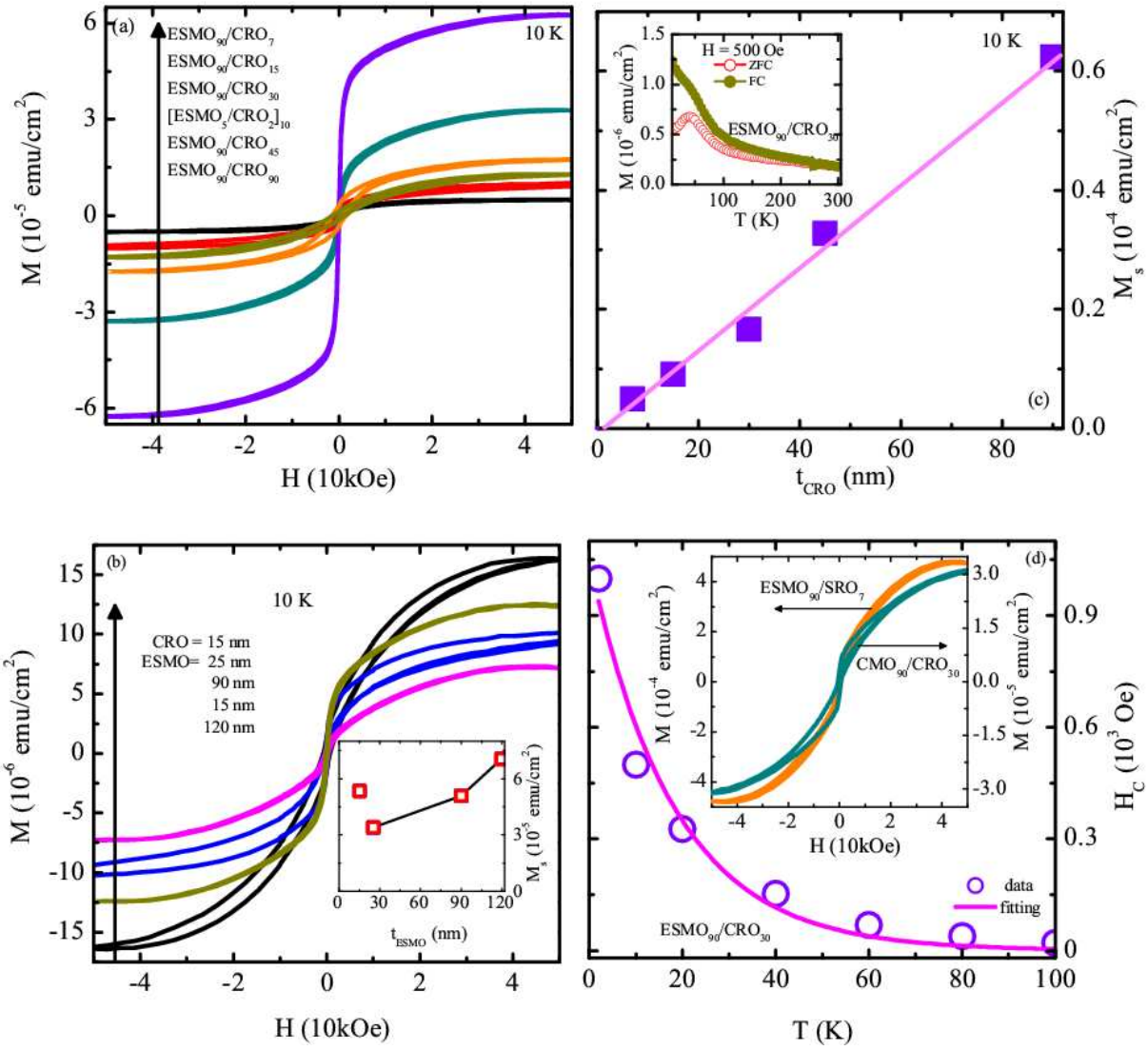

Figure 3: (a & b) Field (H) dependent magnetization (M) at 10 K for $ESMO_{90}/CRO_n$ (n = 7, 15, 30, 45, 90nm) bilayers, $[ESMO_5/CRO_2]_{10}$ multilayer and $ESMO_m/CRO_{15}$ (m = 120, 90, 25, 15 nm) bilayers, respectively. (c) The saturation magnetization (M_s) as a function of CRO thickness (t_{CRO}) and inset in 'c'shows a typical temperature (T) dependence of M data in zero-field-cooled (ZFC) and field-cooled (FC) protocols, while inset in 'b' shows M_s versus ESMO layer thickness (t_{ESMO}). (d) Coercivity (H_C) at various temperatures (symbols) for $ESMO_{90}/CRO_{30}$ and dashed line is fit for $ESMO_{90}/CRO_{30}$, with the equation $H_C(T) = H_C^0 e^{(-T/T_A)}$. Inset (d) is the M-H plot of CMO_{90}/CRO_{30} and $ESMO_{90}/SRO_7$ bilayers.

Nanoscale Accepted Manuscript

View Article Online
DOI: 10.1039/C4NR07314B

Published on 12 January 2015. Downloaded by Selcuk University on 14/01/2015 15:24:18.

Figure 4:

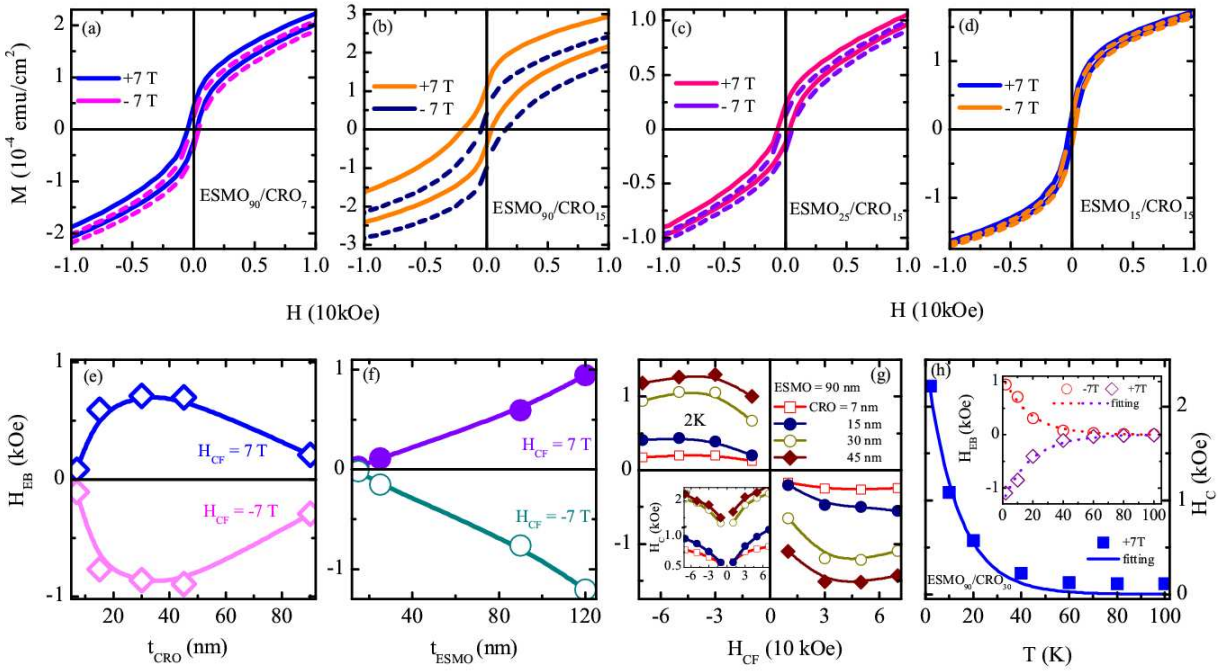

Figure 4 : Field (H) dependent magnetization (M) at 10 K for (a & b) $ESMO_{90}/CRO_n$ (n = 7, 30 nm) and (c & d) $ESMO_m/CRO_{15}$ (m = 25, 15 nm) bilayers upon cooling in a field (H_{CF}) of ± 7 T from 250 K. (e & f) the CRO thickness (t_{CRO}) and ESMO thickness (t_{ESMO}) dependence of exchange-bias field (H_{EB}), respectively, at 10K in ± 7 T cooling field. (g) H_{CF} dependence of H_{EB} and 'inset g' coercive field (H_C) for $ESMO_{90}/CRO_n$ bilayers at 2K. (h) H_C at various temperatures at cooling field + 7 T for $ESMO_{90}/CRO_{30}$ bilayer. Dashed line is fit of H_C-T, with the equation $H_C(T) = H_C^0 e^{(-T/T_A)}$. Inset (h) depicts H_{EB} at various temperatures for $ESMO_{90}/CRO_{30}$ bilayer and dashed lines are fits, with the equation $H_{EB}(T) = H_{EB}^0 e^{(-T/T_A)}$.

Nanoscale Accepted Manuscript

View Article Online
DOI: 10.1039/C4NR07314B

Published on 12 January 2015. Downloaded by Selcuk University on 14/01/2015 15:24:18.

Figure 5:

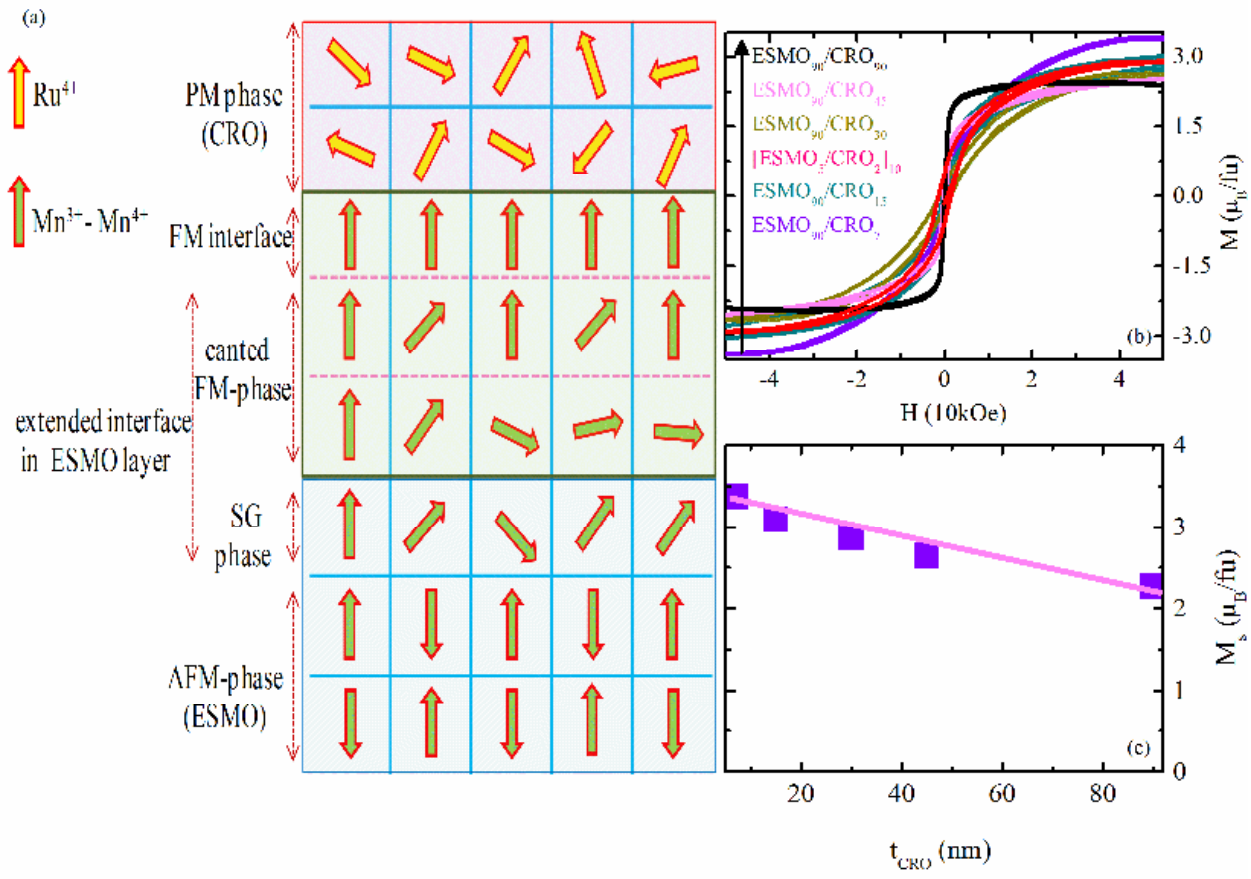

Figure 5: (a) Schematic structure of the $Eu_{0.42}Sr_{0.58}MnO_3/CaRuO_3$ bilayer interface, indicating a ferromagnetic (FM) arrangement of spins at the bilayer inetrafce and the canted FM spins + spin glass (SG) like arrangement in the interfacial layer which is extended into the 2-3 layers of $Eu_{0.42}Sr_{0.58}MnO_3$ part due to the electron leakage. (b) Field (H) dependent magnetization (M) at 10 K for $ESMO_{90}/CRO_n$ (n = 7, 15, 30, 45, 90nm) and $[ESMO_5/CRO_2]_{10}$ bilayers, respectively. (c) The saturation magnetization (M_s) as a function of CRO thickness (t_{CRO}).

Nanoscale Accepted Manuscript

View Article Online
DOI: 10.1039/C4NR07314B

Published on 12 January 2015. Downloaded by Selcuk University on 14/01/2015 15:24:18.

Figure 6:

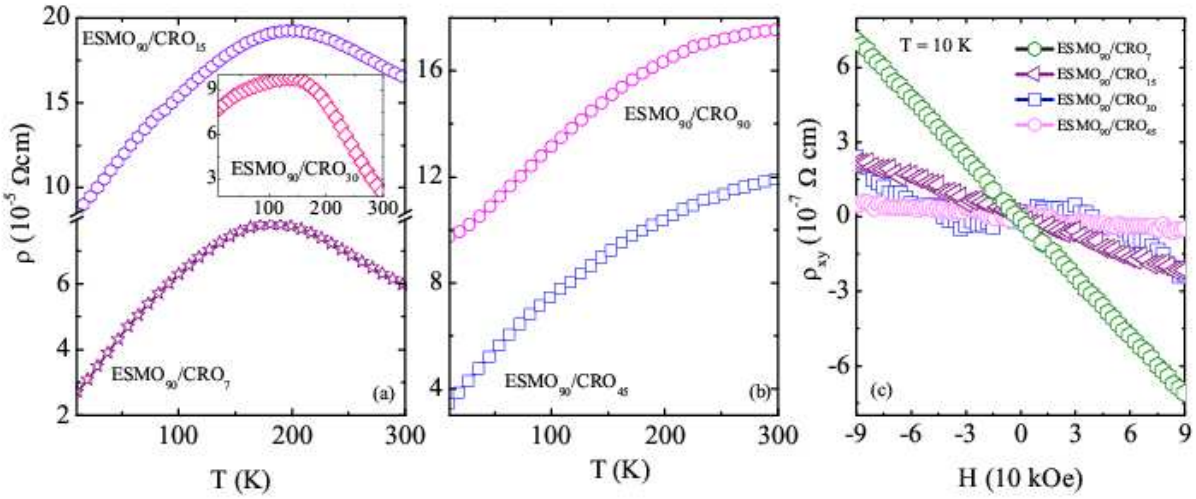

Figure 6: Temperature (T) dependence of resistivity (ρ) in heating protocol for $ESMO_{90}/CRO_n$ bilayers for (a) n = 7 and 15 nm, inset (a) n = 30 nm and (b) n = 45 and 90 nm. (c) H dependence of Hall resistivity (ρ_{xy}) for $ESMO_{90}/CRO_n$ (n = 7, 15, 30, 45 nm).

Nanoscale Accepted Manuscript